Preprint
UCRL-JC-147516

Electron Cloud Effects in Intense, Ion Beam Linacs Theory and Experimental Planning for HIF

A.W. Molvik, R.H. Cohen, S.M. Lund, F.M. Bieniosek, E.P. Lee, L.R. Prost, P.A. Seidl, J.L. Vay

This article was submitted to: 14h International Symposium on Heavy Ion Inertial Fusion, Moscow, Russia

May 2002

U.S. Department of Energy

Lawrence
Livermore
National
Laboratory

DISCLAIMER

Electron cloud effects in intense, ion beam linacs theory and experimental planning for heavy-ion fusion

A. W. Molvik,* R. H. Cohen,† S. M. Lund,† F.M. Bieniosek,‡ E.P. Lee,‡ L.R. Prost,‡ P.A. Seidl,‡ and Jean-Luc Vay‡
Heavy-Ion Fusion Virtual National Laboratory
(Dated: May 18, 2002)

Heavy-ion accelerators for heavy-ion inertial fusion energy (HIF) will operate at high aperture-fill factors with high beam current and long durations. (Injected currents of order 1 A and 20 μs at a few MeV for each of ~100 beams, will be compressed to the order of 100 A and 0.2 μs, reaching GeV energies in a power plant driver.) This will will be accompanied by beam ions impacting walls, liberating gas molecules and secondary electrons. Without special preparation, the ~10% electron population predicted for driver-scale experiments will affect beam transport; but wall conditioning and other mitigation techniques should result in substantial reduction. Theory and particle-in-cell simulations suggest that electrons, from ionization of residual and desorbed gas and secondary electrons from vacuum walls, will be radially trapped in the ~4 kV ion beam potential. Trapped electrons can modify the beam space charge, vacuum pressure, ion transport dynamics, and halo generation, and can potentially cause ion-electron instabilities. Within quadrupole (and dipole) magnets, the longitudinal electron velocity is limited to drift velocities ($E \times B$ and ∇B) and the electron density can vary azimuthally, radially, and longitudinally. These variations can cause centroid misalignment, emittance growth and halo growth. Diagnostics are being developed to measure the energy and flux of electrons and gas evolved from walls, and the net charge and gas density within magnetic quadrupoles. We will also measure the depth of trapping of electrons, their axial and radial transport, and the effects of electrons on the ion beam.

I. INTRODUCTION

Electron clouds have limited the performance of many positive beam rings [1–3]. We have initiated a program to determine whether they can also be dangerous in a linac. There are three main reasons for concerns with heavy-ion fusion (HIF) induction linacs: HIF injectors produce beams with line charges of ~0.2 μCoul/m resulting in several kilovolt beam potentials, which can strongly confine electrons; injected pulses have a flattop duration of ~20 μs which allows time for gas desorbed from walls by beam halo to reach the beam; and finally HIF has an economic incentive to minimize induction-core mass by fitting beam tubes tightly to the beams; how tightly may be limited by the increased generation of gas and electrons from ion bombardment of walls and reduced time for these to reach the beam.

Induction accelerators were chosen by the USA program to develop as drivers for HIF inertial fusion energy power plants because they are capable of accelerating beams currents of 10^2 to 10^4 A that are required to deliver several megajoules of energy to a target with GeV range ions [4]. In induction accelerators, the axial acceleration gaps between beam-tube arrays are surrounded by induction cores. The core mass can be reduced by reducing the diameter of the multiple beam array inside the cores, allowing smaller inner and outer core diameters for the same cross-sectional area (therefore the same volt-seconds from Faraday's Law). Reducing the beam tube diameters is beneficial because the total mass of induction cores in an inertial fusion power plant is predicted to be in the range of 10-30 $\times$ 10^6 kg, making this a major cost area [5]. HIF induction accelerators are at an early stage of development. The parameters listed in this paper represent todays concepts, which are expected to evolve.

Heavy-ion beams will be injected with about 20 μs flat top duration, and with rise and fall times of a fraction of a microsecond [5]. To maintain the flattop against space-charge driven longitudinal expansion, rapidly ramped-pulses are applied at frequent intervals to the head of the beam to slow ions there and to the tail of the beam to accelerate lagging ions. As the beams are accelerated, other ramped pulsers place a velocity tilt on them, to compress their duration and to maintain the beam current near the transport limit of magnetic quadrupoles. Minimizing the pulse duration increases the cost effectiveness of induction acceleration, providing the required volts of acceleration from a smaller volt-seconds cross-sectional area of induction cores. [New concepts are desirable for injection and low-energy transport, that would allow use of higher beam currents for shorter durations (and possibly in fewer beams) to inject the required number of ions. Such concepts would further reduce the mass of induction cores in a driver.]

The behavior of electrons in these flattopped beams will be similar to those in filled storage rings. In particular, the multipactor mechanism for electron generation and acceleration by bunched beam trains should not be present [1]. Ionization of gas is expected to be the domi-

*molvik1@llnl.gov; Lawrence Livermore National Laboratory, Livermore, CA 945500, USA
†Lawrence Livermore National Laboratory, Livermore, CA 945500, USA
‡Ernest Orlando Lawrence Berkeley National Laboratory, 1 Cyclotron Road, Berkeley, CA 94720, USA

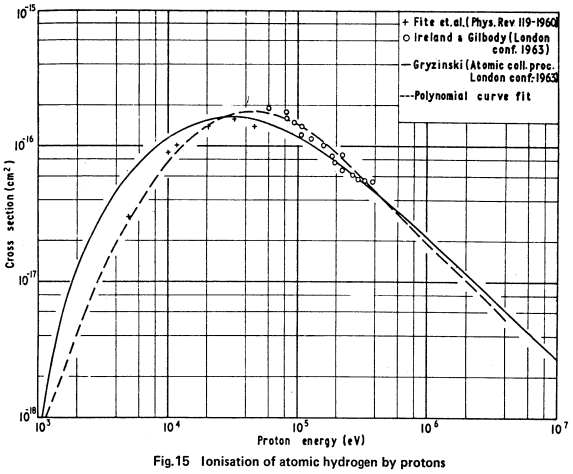

FIG. 1: The cross section for the ionization of atomic hydrogen by protons is shown as indicative of approximate ionization cross sections for typical background and adsorbed gases in vacuum systems, when heavy ion beam energies are normalized to the energy per nucleon [6].

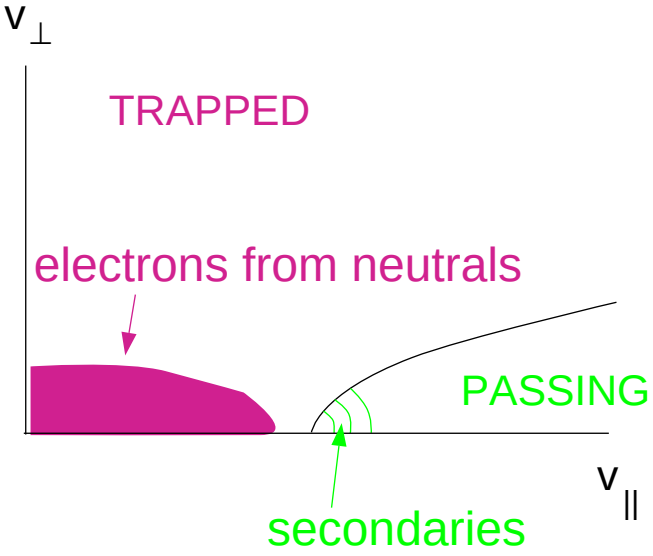

FIG. 2: (Color) Velocity space diagram of electron confinement in a magnetic field, shown at the potential peak on the beam axis. Secondary electrons from the wall are born untrapped, and can be weakly trapped by non-adiabaticity or instabilities. Electrons from the ionization of gas by collision with beam ions are born trapped, the depth of trapping depends on the radial location of the ionization event.

nant electron source term that leads to trapped electrons.

The present HIF experiments use potassium ion beams at energies of 0.5-1.8 MeV. The High-Curent Experiment (HCX) is studying coasting K^+ beams injected with 0.2-0.5 A at 1.0-1.8 MeV, these energies corresponding to 25-45 keV/nucleon. The peak beam potential will range from 2 to 4.5 kV, and the flattop duration is currently 4 μs, with rise and fall times in the range of 1 μs.

The interaction of HCX beams with gas is expected to be similar to that of a proton beam with atomic hydrogen gas, as shown in Fig. 1 [6]. The present range of energies, 25-45 keV/nucleon is near the peak cross section for ionization of background gas. Above ~200 keV/nucleon, the cross sections decrease almost linearly with beam energy. For HIF, the maximum energy needed at the target is in the range of 10-20 MeV/nucleon [7], where the cross sections are two orders of magnitude below the peak. High-energy physics accelerators typically are three to six orders of magnitude higher than this in beam energy per nucleon, with ionization cross sections nearly three to six orders of magnitude smaller than the minimum in HIF drivers.

II. THEORY - INITIAL RESULTS

We have studied the confinement of electrons by positive potential particle beams primarily within a series of quadrupole magnets. It became apparent that the electron confinement by a beam in quadrupole magnets is similar to that in our previous studies of electron confinement by magnetic-mirror confined, hot-ion plasmas [8, 9].

Electrons in a magnetic field will have a conserved magnetic moment, if they have a gyroradius which is small compared with the gradient scale length of the magnetic field. The magnetic moment is given by

$$\mu = \frac{v_\perp^2}{2B} \qquad (1)$$

where $v_\perp$ is the electron velocity perpendicular to the magnetic field of magnitude B. As a result, electrons which, at the minimum-field-strength point along a field line, have large pitch angles and/or low energies, are confined by the combination of electrostatic and magnetic fields, as shown in Fig. 2. Electrons born at the walls (secondaries) have high energy and small pitch angle at the field minimum, and so are untrapped; electrons born in the beam interior (from ionization of neutrals) are born electrostatically trapped.

This picture is only approximately correct, as electrons in a quadrupole magnetic field undergo jumps in the magnetic moment. These are negligible for field lines far from the axis. But untrapped electrons that pass moderately close to the axis can get trapped by this process and remain so for up to several hundred bounce times, ~1 μs.

In magnetic fields, high enough that the electron gyroradius is small compared with the beam and tube radii, the flow of electrons parallel to the magnetic field is at the kinetic velocity, modified by conservation of the magnetic moment, Eq. 1. The flow of electrons perpendicular to the magnetic field is restricted to the sum of the $E \times B$ and ∇B velocities. In a uniform magnetic field with no electric field, the electron orbit projection on a plane normal to B would be closed circles. An electric field or a

magnetic field gradient opens these circles, resulting in a net drift velocity. These drift velocities are given by

$$v_{E\times B} = \frac{E \times B}{B^2} \tag{2}$$

and

$$v_{\nabla B} = \frac{m}{qB^4}\left(v_{\|}^2 + \frac{v_{\perp}^2}{2}\right)\left[B \times \nabla\frac{B^2}{2}\right] \tag{3}$$

where we have included the curvature drift ($v_{\|}^2$ term) along with the usual ∇B drift ($v_{\perp}^2$ term). In drift regions between quadrupoles, electron confinement is purely by the beam potential.

Electrons generated within the beam by ionization of gas are born trapped as noted above. These will accumulate until the end of the beam pulse. This process, in conjunction with gas released from walls by ion impact, is expected to lead to a significant electron density. We expect that untrapped, secondary electrons from the wall, with trapping only from jumps in magnetic moment near the quadrupole-field nulls, will not build up to sufficiently high densities to significantly impact beam performance. However, if electron-electron instabilities reach significant levels, they could cause much greater trapping of secondary electrons.

The details of the electron transport will differ between drift and magnetic quadrupole field regions. For a flattopped beam within a drift region, we expect the electron density to equilibrate axially, and azimuthally. Radially, electrons will be confined within the birth radius. Within a quadrupole magnet, electron transport is limited to the sum of the ∇B and $E \times B$ drift velocities, directed parallel or antiparallel to the beam, depending on the quadrupole quadrant. The drift velocities are a fraction of the beam directed velocity in HCX, requiring a fraction of a microsecond to drift the 31 cm length of a quadrupole magnet. An electron may drift through multiple magnetic quadrupoles during the flattop beam duration of 4 μs.

Our present experiments also transport beams with electrostatic quadrupoles. In these, the applied electric fields dominate over the beam self fields, so no electron trapping is possible. An increase in the current of single-pass electrons during the pulse is still possible from an increase in gas density due to desorption. Approximates 1% of gas within the beam is ionized and expelled from the beam. Electrostatic quadrupole effects will not be discussed further here.

Electrons reaching a drift region rapidly free-stream to the next magnet where they either bounce back, or enter the next magnet, depending on the local drift velocity direction of that magnet. Those that bounce back to the first magnet continue to bounce until they drift azimuthally to where one of the magnets will accept them. Axial transport of electrons through a series of magnets during the flattop beam duration of 4 μs could be treated as a diffusion process.

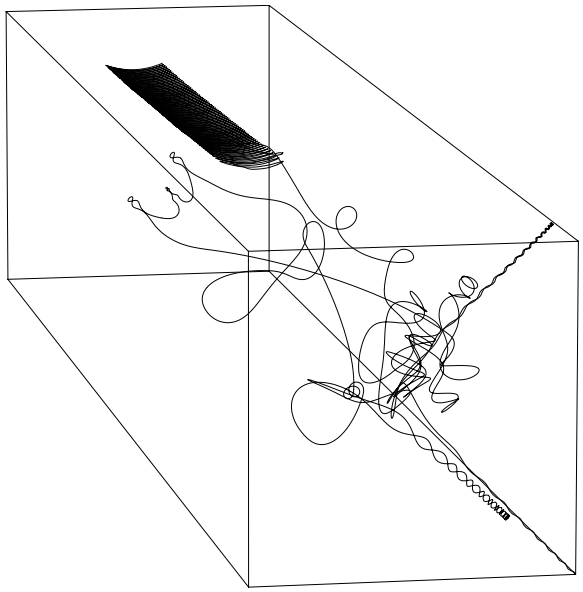

FIG. 3: 3-D plot of initially deeply trapped electron, which ∇B and $E \times B$ drifts slowly through a magnetic quadrupole, starting from the left. It is accelerated across a drift space, bounces between quadrupoles at few times, then enters the upstream (ion beam frame) quadrupole and is lost radially to the wall.

This situation is significantly changed by an acceleration gap within a drift region. It accelerates electrons backwards across an upstream (beam reference) acceleration gap, or reflects them back to the magnet from an acceleration gap at the downstream end of the magnet. Electrons that gain kinetic energy exceeding the potential trapping energy can be detrapped and deflected to the wall by an upstream magnet, Fig. 3. This is the only mechanism we have identified that will cause deeply trapped electrons to be lost before the end of the beam pulse.

The electron particle balance has two main terms, for electrons from ionization of neutrals and for those due to secondary electrons from the wall. The first term for the electron density n_e is given in terms of the neutral density within the beam n_n, the beam density n_b and velocity v_b, the ionization cross section σ, and the electron confinement time τ_e which is generally infinity during the beam flattop (i.e., the electrons remain confined radially by the beam in either drift or magnetized region unless they reach acceleration gaps where they can be accelerated to kinetic energies exceeding the potential well depth).

$$\frac{dn_e}{dt} = n_n n_b \langle \sigma v_b \rangle - \frac{n_e}{\tau_e} \tag{4}$$

where

$$n_n = \frac{2}{r_w}\langle n_{bw} v_{\perp w} \kappa_n \rangle (t - \tau_{nw}) \tag{5}$$

for a wall radius r_w, a beam density n_{bw} and velocity $v_{\perp w}$

at the wall, a gas desorption coefficient κ_n in molecules per incident beam ion, and the time of flight of gas from the wall to the beam τ_{nw}. We expect electron densities to reach several percent by the end of a 4 μs pulse in a background vacuum of 10^{-7} torr. Desorbed gas from the wall will increase electron densities further.

The trapping of secondary electrons originating at the wall radius r_w is given in terms of number of bounces that an electron is trapped Λ, the secondary emission yield κ_e, and the electron bounce time τ_{ew} which is typically 3-4 ns. We have also included a term due to photo-electrons with a coefficient κ_ν, the photons are from exitation by beam-gas collisions $\sigma_\nu v_b$, and are thought to be a small effect.

$$\frac{dn_e}{dt} = \frac{n_{bw}}{n_b}\frac{v_{\perp w}}{v_b} n_b \langle\Lambda\rangle \frac{v_b}{r_w}\kappa_e + n_n n_b \langle\sigma_\nu v_b\rangle \kappa_\nu - \frac{n_e}{\langle\Lambda\tau_{ew}\rangle} \quad (6)$$

We expect electron densities from this effect to be much less than 1%, averaged over the beam.

III. HCX FACILITY

Electron cloud experiments in HCX will be primarily performed with four pulsed magnetic quadrupoles. Each magnet has coil lengths of 31 cm, a gradient of up to 16 T/m, and a half-lattice length of 52 cm, including 4.3 cm for diagnostic access between each pair of quadrupoles. Each quadrupole has an elliptical bore with 3 × 5 cm radii at the center [10].

These provide a range of operation from transporting a small diameter beam, with an envelope radius about half that of the walls – minimizing electron and gas generation, to transporting a beam whose envelope approaches or scrapes the walls – maximizing electron and gas generation. Such a range is shown in Fig. 4. To determine limits, we will vary beam operation, until enough beam scrapes the walls to significantly change beam performance or produce electron densities approaching the beam density. Other envelope solutions (not shown) produce matched transport through the last two magnetic quadrupoles after expanding to significantly larger radius in the first magnetic quadrupole, these can produce solutions with small radii in the last two quadrupoles, but cannot attain large radius solutions there.

Before the quadrupole magnets are installed, we will begin measurements with the Gas-Electron Source Diagnostic (GESD), Fig. 5. It will be located at the end of the diagnostics tank 1.3 m beyond the end of the quadrupole transport. This drift distance will allow the beam to expand to a diameter of ∼15 cm. An entrance aperture of 0.3 × 2.5 cm allows ∼0.4% of the beam current into a box where it will impact a target at 75-88° from normal incidence. An ion gauge will measure the peak pressure rise, from which we will determine the total gas desorbed from the target. The gas pressure in the box will decay with a time constant of ∼0.5 s through pumpout holes, which is adequate for the HCX rate of 1 pulse every 10 s.

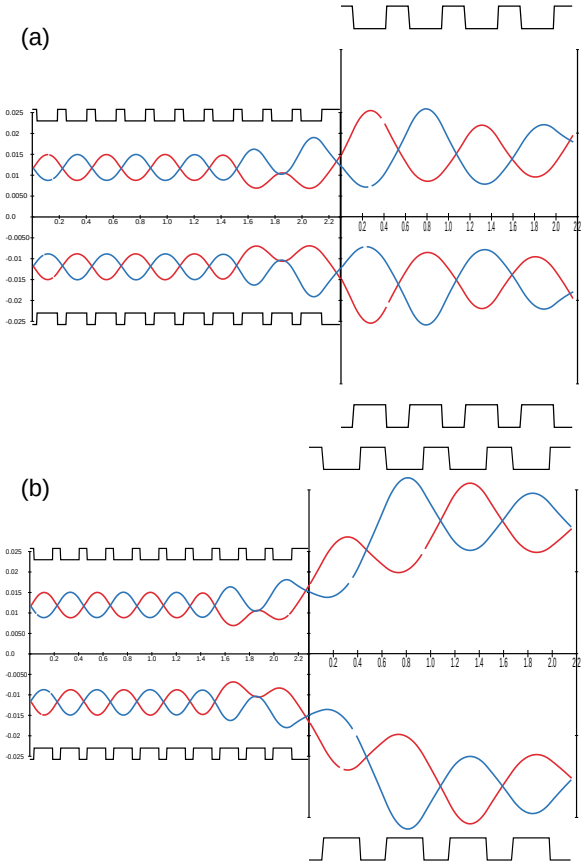

FIG. 4: (Color) Transport of a 1.0 MeV K^+ beam through 10 electrostatic quadrupoles on the left, a short drift space for diagnostics including slit scanners, followed by 4 magnetic quadrupoles. (a) A minimum radius beam is transported through the magnetic quadrupoles. (b) One of a large class of beam envelopes that approach or scrape the walls in the magnetic quadrupoles.

The target, catcher, and a surrounding grid in the GESD can be independently biased relative to the walls, to measure the current and energy of either secondary electrons or low energy secondary ions (up to a few hundred eV), and to determine the beam current to the target. At angles approaching 88°, TRIM Monte-Carlo calculations [11] predict that up to 70% of the incident ions will be reflected back out of the target, most of which will hit the ion-catcher at near normal incidence where they will stick and will not be reflected again. For 1.8 MeV beam ions incident at 88° from normal, 80% of ions scattered off the wall are at angles of less than 0.35 rad, with only 10% at angles greater than 0.5 rad. The purpose of the ion catcher is to reduce the number of ions scattered into the grid where they will produce secondary electrons, some of which will reach the target. We must keep this secondary electron current small, so that the error, in the measured beam current to the target, will be small.

The energies of desorbed molecules can also be measured – the wall beyond the ion gauge can be opened, in-

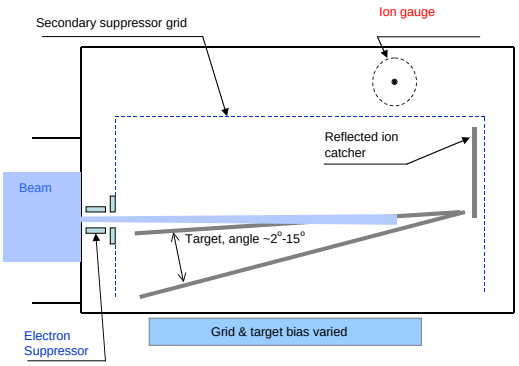

FIG. 5: (Color) The Gas-Electron Source Diagnostic (GESD) measures the number of energy of electrons and gas moelcules per incident K^+ ion. It can calibrate secondary electron measurements to beam loss and gas desorption, and can evaluate mitigation techniques.

FIG. 6: An array of collectors is shown; from left to right is (a) a flush collector, (b) a recessed collector or capacitive probe, (c) a 1-grid, and (d) a 2-grid collector.

creasing the time for gas molecules to reflect back to the gauge. Then the time of flight of molecules in the range of a few to a few hundred microseconds can be measured. This will enable us to estimate the time for gas to cross a gap between the beam and a wall, from which we can estimate the maximum beam duration that is unaffected by wall reflux. The main portion of the beam is caught in a 15 cm diameter, 23 cm long tube extending out from the beam entrance aperture. The gas from the main portion of the beam will take a few hundred microseconds to flow out and around the tube, reach the ion gauge and dominate the measurement. Time-of-flight measurements are valid only before this time. Electron (and gas) reduction techniques will be evaluated with the GESD.

We evaluated various diagnostics (Fig. 6) to measure and distinguish secondary electrons due to beam ions impinging on the wall (and to scattered ions resulting from beam ions impinging on the opposite wall), photo-electrons, ions from gas that are expelled with kinetic energy equal to the beam potential at their birth point, and untrapped electrons. A collector at the wall-potential, flush with the surface, measures the net current of all these particles, but can't distinguish between them. A second collector is recessed so that most primary and reflected beam ions can't reach it, but the other particles and electric field can; the difference between the two will be the beam current plus the secondary electron current.

Simple gridded collectors measure the remaining electron sources. A collector, shielded by 1-grid, measures the sum of the current of ions from gas plus untrapped electrons. The grid and collector are recessed so that few scattered ions reach them, since secondary electrons that reach the backside of the grid will be collected. A positive collector bias suppresses photo-electrons. A grounded collector with 2-grids, the second biased to repel electrons, measures the ionization current expelled by the beam. This directly gives the source of ions from ionization of gas. It is closely related to the source of deeply trapped electrons but includes charge exchange as well as ionization of gas. It can also be calibrated to measure the gas pressure within the beam as a function of time. The source term for expelled ions is closely related to the source term for electrons but it includes charge exchange as well as ionization. The time is skewed by the time-of-flight of the ions to the collector which is in the range of a few tenths of a microsecond for potentials of a few kV and ion masses near 20 AMU. This analyzer will also be operated in a mode to measure electron energies, as developed by the ANL group [12]. If instability levels are low, as we currently expect, the escaping electrons will have low energies of a few eV.

The escaping electron current will be especially informative during the at the end of the pulse when the confining potential of the beam decreases with the beam current. Then in Fig. 2, the loss boundary will move towards the origin, causing weakly trapped electrons that originated as secondary electrons at the wall, to be lost first. For a beam envelope that is well separated from the wall, we then expect a gap in the electron loss current until the beam potential decreases sufficiently for the much-more deeply-trapped electrons from ionized gas to be lost. Plotting the electron current versus the change in beam potential from the flat-top gives the depth-of-trapping energy distribution for electrons, and the integrated electron charge will give the accumulated trapped electron charge (per unit length and azimuth) at the end of the beam flattop. The difference between the total deeply-trapped electron charge and the integrated ion source term from the 2-grid collector provides an experimental estimate of charge-exchange versus ionization.

We plan two methods to measure the beam potential: (1) Capacitive probes, recessed with no grid, measure the electric field near the wall, from which the peak potential can be determined. (2) A gridded energy analyzer (GEA) [13, 14] measures the energy distribution of ions (from gas) that are expelled from the beam. Capacitive probes are very simple, in arrays they are used as beam-position monitors to determine the centroid, ellipticity, and perhaps the tilt of beams. The major uncertainty arises from particle and photon bombardment of the capacitive plate – the plate can be shielded from direct beam bombardment, and most scattered beam ions, by recessing it behind another electrode; however, untrapped electrons, expelled ions, and photons cannot be

prevented from bombarding the surface. Their currents, together with secondary production, add to the capacitive charging and discharging currents that occur during the rise and fall of the beam current.

The GEA consists of three grids preceding the collector: a grounded entrance grid, an ion repeller grid, and an electron repeller grid. The novel aspect of this analyzer is the requirement of biasing the ion repeller grid up to ∼5 kV. The ion-repeller precedes the electron repeller so that secondary electrons produced by reflected ions striking the back of the preceding grid will be stopped by the subsequent electron repeller grid, and so the electron repeller grid can also function as a secondary suppresser grid for the collector [13]. This arrangement can also be operated to measure photo-electrons off the collector [14]. We are also investigating the possibility of purchasing an ion energy and mass resolving analyzer from the A. F. Ioffe Physical-Technical Institute, St. Petersburg, Russia [15]. This instrument is called the Compact Ionized Particles Analyzer (CIPA), based on a similar unit developed for analyzing the flux of energetic neutral flux (to 160 keV hydrogen or 4 keV argon), resulting from energetic ions that charge-exchange on neutral atoms, in magnetic fusion experiments. It can resolve 1 AMU mass differences up to about 44 AMU.

In summary, we have listed a variety of simple instruments with which we will begin the quantitative study of the electron-cloud particle balance, the variation of electron-cloud parameters with the fill-factor of the beam in the beam tube, wall conditioning and other mitigation techniques, and – with the use of standard beam diagnostics – the effect of electrons on beam performance in HIF driver-scale beams.

Acknowledgments

We are grateful to Grant Logan for support and encouragement in this work, and to Miguel Furman for stimulating discussions connecting us to the main body of e-cloud work. This work was performed by the University of California Lawrence Livermore National Laboratory under the auspices of the U.S. Department of Energy under contract No. W-7405-ENG-48 and Lawrence Berkeley National Laboratory DE-AC03-76F00098.

[1] K. Ohmi, Phys. Rev. Lett. **75**, 1526 (1995).
[2] M. A. Furman and G. R. Lambertson, in *Proc. of the International Workshop on Multibunch Instabilities in Futhre Electron and Positron Accelerators*, edited by P. L. Roux, J. Poole, and M. Truchet (KEK Proceedings 97-17, 1997, Tsukuba, 1997), p. 170.
[3] G. Rumolo, F. Ruggiero, and F. Zimmermann, Phys. Rev. ST-AB **4**, 012801 (2001).
[4] R. O. Bangerter, Nuovo Cimento **106**, 1993 (1993).
[5] W. R. Meier, J. J. Barnard, and R. O. Bangerter, Nucl. Instr. and Meth. A **464**, 433 (2001).
[6] R. L. Freeman and E. M. Jones, Tech. Rep. CLM-R 137, Culham Laboratory, Abingdon Berkshire (1974).
[7] D. A. Callahan-Miller and M. Tabak, Nucl. Fusion **39**, 883 (1999).
[8] D. E. Baldwin, Rev. Mod. Phys. **49**, 317 (1977).
[9] R. F. Post, Nuclear Fusion **27**, 1579 (1987).
[10] A. Faltens, N. Y. Li, G. Ritchie, and D. Shuman, Proceedings of the 1999 Particle Accelerator Conference p. 3339 (1999).
[11] J. F. Zielgler, J. P. Biersack, and U. Littmark, *The Stopping and Range of Ions in Solids* (Pergaman Press, New York, 1985).
[12] R. A. Rosenberg and K. C. Harkay, Nucl. Instr. and Meth. A **453**, 507 (2000).
[13] A. W. Molvik, Rev. Sci. Instrum. **52**, 704 (1981).
[14] C. Bohm and J. Perrin, Rev. Sci. Instrum. **64**, 31 (1993).
[15] mpetrov@npd.ioffe.rssi.ru (2002), Private communication.

University of California
Lawrence Livermore National Laboratory
Technical Information Department
Livermore, CA 94551